

# Modeling granular phosphor screens by Monte Carlo methods

Panagiotis F. Liaparinis

*Department of Medical Physics, Faculty of Medicine, University of Patras, 265 00 Patras, Greece*

Ioannis S. Kandarakis and Dionisis A. Cavouras

*Department of Medical Instruments Technology, Technological Educational Institute, 122 10 Athens, Greece*

Harry B. Delis and George S. Panayiotakis<sup>a)</sup>

*Department of Medical Physics, Faculty of Medicine, University of Patras, 265 00 Patras, Greece*

(Received 9 December 2005; revised 30 September 2006; accepted for publication 2 October 2006; published 8 November 2006)

The intrinsic phosphor properties are of significant importance for the performance of phosphor screens used in medical imaging systems. In previous analytical-theoretical and Monte Carlo studies on granular phosphor materials, values of optical properties, and light interaction cross sections were found by fitting to experimental data. These values were then employed for the assessment of phosphor screen imaging performance. However, it was found that, depending on the experimental technique and fitting methodology, the optical parameters of a specific phosphor material varied within a wide range of values, i.e., variations of light scattering with respect to light absorption coefficients were often observed for the same phosphor material. In this study, x-ray and light transport within granular phosphor materials was studied by developing a computational model using Monte Carlo methods. The model was based on the intrinsic physical characteristics of the phosphor. Input values required to feed the model can be easily obtained from tabulated data. The complex refractive index was introduced and microscopic probabilities for light interactions were produced, using Mie scattering theory. Model validation was carried out by comparing model results on x-ray and light parameters (x-ray absorption, statistical fluctuations in the x-ray to light conversion process, number of emitted light photons, output light spatial distribution) with previous published experimental data on  $\text{Gd}_2\text{O}_2\text{S}:\text{Tb}$  phosphor material (Kodak Min-R screen). Results showed the dependence of the modulation transfer function (MTF) on phosphor grain size and material packing density. It was predicted that granular  $\text{Gd}_2\text{O}_2\text{S}:\text{Tb}$  screens of high packing density and small grain size may exhibit considerably better resolution and light emission properties than the conventional  $\text{Gd}_2\text{O}_2\text{S}:\text{Tb}$  screens, under similar conditions (x-ray incident energy, screen thickness). © 2006 American Association of Physicists in Medicine. [DOI: 10.1118/1.2372217]

Key words: x-ray imaging, phosphor screens, Monte Carlo, modeling, MTF

## I. INTRODUCTION

Luminescent materials are employed as radiation to light converters in detectors of medical imaging systems.<sup>1–3</sup> In x-ray projection imaging, a large number of such materials have been employed in the form of granular screens,<sup>4</sup> often referred to as phosphor screens, consisting of a large number of grains embedded within a binding material. The x-ray detection and imaging performance of phosphor screens are affected by intrinsic physical properties, related to x-ray and light photon transport through the material. These properties have been previously investigated by experimental,<sup>5–11</sup> theoretical,<sup>11–15</sup> and Monte Carlo methods,<sup>16–22</sup> and have been taken into account in the design of commercial imaging systems.<sup>23–25</sup>

Phosphor screens have been previously<sup>12,14,15,26–30</sup> modelled as a series of superimposed x-ray absorbing, light creating, and light attenuating elementary thin layers within the framework of cascaded linear systems analysis. Analytical methods, based on photon diffusion equations or on one-dimensional light transport considerations,<sup>14,15,26–29</sup> have been preferably employed to investigate phosphor intrinsic

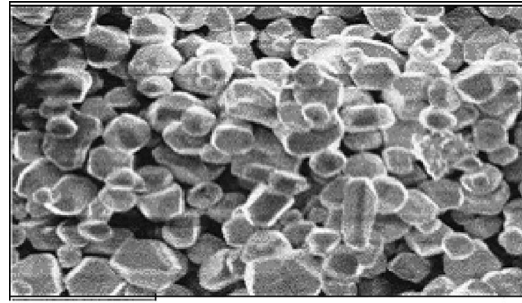
properties. Analytical and recursive methods have also been used to model phosphor screens as an ensemble of grains of specific size.<sup>31,32</sup> On the other hand, most Monte Carlo studies<sup>20,21,33–35</sup> have focused on the simulation of x-ray interactions within the phosphor's mass, mainly using available Monte Carlo simulation packages.<sup>33–35</sup> Only a few Monte Carlo studies have investigated or have taken into consideration the effects of phosphor screen light transport properties. Morlotti<sup>36</sup> has employed Monte Carlo methods to evaluate the emission efficiency and the modulation transfer function of phosphor screens by taking into consideration light propagation effects. Radcliffe *et al.*<sup>37</sup> and Kausch *et al.*<sup>38</sup> have studied light transport in phosphor screens for portal imaging applications. They have used a Monte Carlo code, based on Fresnell reflection at phosphor grain boundaries. Most recently, Badano *et al.*<sup>39</sup> have used light attenuation (scattering and absorption) coefficients to study, via the DETECT II Monte Carlo simulation code, the signal and noise transfer and the so-called Lubberts effect in columnar and granular screens. In all these studies, light propagation has been examined using optical parameters determined either by empirical methods or by fitting to experimental

data.<sup>14,15,26–30,39</sup> This may be inconvenient, since for predicting the performance of a phosphor material one has to prepare screens and perform measurements or, otherwise, to use experimental data obtained by others on already prepared screens.

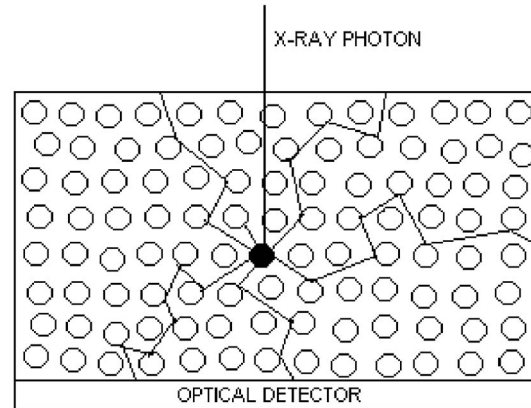
In currently employed granular screens, phosphor grains are glued together by a binding material in a close-packed spatial distribution. This distribution is described by the screen packing density, expressing the active phosphor volume over the total screen volume, which in conventional screens is of the order of 50%. However, in the last decade, new performance boosting phosphor screen preparation techniques have been introduced, such as sintering techniques, for preparing ceramic plates that in effect increase the densification (packing density) in luminescent materials.<sup>4,40</sup> To our knowledge, the influence of that higher packing density on the imaging performance of phosphor screens has not yet been investigated systematically.

In the present study, phosphor screen performance was investigated under diagnostic radiology conditions utilizing a custom Monte Carlo simulation code developed in MATLAB. The latter only requires, as input data, standard reference tabulated data of the phosphor material's intrinsic parameters (x-ray interaction parameters, x-ray to light conversion efficiency, light wavelength, complex refractive index) and structural parameters (grain size and packing density). In particular, the simulation code was developed by performing a detailed account of the following: (i) The energy deposition, and the corresponding contribution to light generation, from the x-ray photon interactions within the diagnostic energy range. This account comprised the elastic and inelastic scattering effects as well as the photoelectric effect including the emission of  $K$  x rays or Auger electron for energies above the  $K$ -absorption edge. (ii) The light generation and the interactions of light photons with the phosphor grains, based on the scattering theory of Mie.<sup>41,42</sup> The model takes into account the contribution of the complex refractive index of the phosphor material in light propagation. This index is closely related to the microscopic light interaction probabilities, which in turn are functions of particle (phosphor grain) size and light wavelength. The model can predict phosphor performance solely by Monte Carlo simulation, without having to prepare screens and perform measurements or use experimental data obtained by others.

The proposed Monte Carlo model was applied to simulate the performance of the well-known commercial,  $\text{Gd}_2\text{O}_2\text{S}:\text{Tb}$  based, Kodak Min-R screen. For this screen, the variation of the x-ray absorption and the light emission properties with x-ray energy were found. Data related to the contribution of each physical process to the emitted light were also derived. The modulation transfer function (MTF) of the screen was predicted and the effect of grain size and phosphor packing density on MTF was studied. Results were validated with respect to previous experimental measurements, under similar conditions.<sup>9,14</sup> In addition, the noise associated with the x-ray to light conversion process, quantified in the Swank factor,<sup>8–10,29</sup> was taken into account and the corresponding detective quantum efficiency (DQE) was estimated. Finally,



(a)



(b)

FIG. 1. (a) Image of  $\text{Gd}_2\text{O}_2\text{S}$  phosphor grains, obtained by electronic microscope. (b) Schematic diagram illustrating a phosphor screen in contact with an optical detector, an x-ray photon interaction (black dot), and generated light photon trajectories (black lines).

a suitable combination of grain size and packing density is proposed, for which the resolution and light emission properties of granular phosphor screens (e.g.,  $\text{Gd}_2\text{O}_2\text{S}:\text{Tb}$ ) become higher, under similar conditions.

## II. MONTE CARLO SIMULATION METHOD

### A. Geometry of the simulation model

The geometry of the simulation model is illustrated in Fig. 1. The phosphor screen was modeled as a three-dimensional layer consisting of uniformly distributed grains. All grains were of the same size, which was assumed to be equal to the mean size of the grains contained in a commercial screen.<sup>31</sup> The simulation code was suitably developed in order to allow changes of the following parameters: phosphor screen (layer) thickness, screen area (surface dimensions), screen packing density, and phosphor grain diameter. X-ray photons with energy either given from a monoenergetic beam or sampled from an x-ray spectral distribution were assumed to impinge on the screen surface according to predefined beam geometries, i.e., narrow beam or parallel beam. In addition, the role of the substrate material, between the phosphor screen and the optical detector, was taken into consideration in the validation procedure.

## B. Required input data to the Monte Carlo program

The input physical data, required for the Monte Carlo simulation program, included the phosphor material's chemical composition, the x-ray photon's spectral distribution, and the numerical values of various physical parameters and coefficients relevant to x-ray interactions and to optical properties of the material. All values were taken from validated tabulated data and libraries. In particular, the parameters and coefficients employed were the following: data relevant to the x-ray spectrum,<sup>43–45</sup> the mass attenuation coefficients of the material,<sup>46–48</sup> the mass partial interaction coefficients of the material,<sup>46–48</sup> the mass partial interaction coefficients of each element of the chemical compound and their fractional weight,<sup>46–48</sup> the incoherent scattering functions,<sup>49</sup> the atomic form factors,<sup>49</sup> the probability of the *K*- or *L*-shell contribution to the photoelectric effect,<sup>47,48,50</sup> the *K*-fluorescent yield<sup>51</sup> for the production of characteristic radiation or the probability of Auger electron production, the *K*- or *L*-shell binding energies,<sup>50</sup> the transition probabilities of atom relaxation,<sup>50</sup> the refractive index of the phosphor material<sup>37,52</sup> and of the medium,<sup>53</sup> the phosphor's intrinsic conversion efficiency,<sup>3</sup> and the wavelength of the emitted light.<sup>3</sup>

## C. X-ray photon history

An x-ray photon history was considered to start when a photon, with energy obtained from the x-ray energy spectrum distribution (or from a monoenergetic beam), impinged on the phosphor screen surface. The x-ray photon was considered to penetrate the screen, and its transport through the phosphor slab was described in terms of the photon free path length (fpl),<sup>21</sup> taking into account the packing density of the phosphor screen. The interaction site coordinates were determined by the fpl and the initial direction of the x-ray photon. The type of interaction was selected according to the relative probabilities of occurrence of each process. Once the type of interaction is selected, the interaction occurs at the corresponding chemical element of the phosphor material.<sup>12</sup>

If the x-ray photon undergoes photoelectric absorption, a sequence of processes may occur depending on its energy  $E$ . When the photon energy is larger than the *K*-shell binding energy  $U_K$ , photoelectric absorption may occur either in the *K*-shell or in the *L*-shell. In the case of interaction in the *K*-shell, the emission of *K*-characteristic radiation or the production of Auger electrons may arise according to the *K*-fluorescent yield  $\omega_K$ . If *K*-characteristic radiation is emitted, the trajectory of the new photon within the phosphor is examined separately. Otherwise, an Auger electron is emitted, which is assumed to be locally absorbed. In this study, the following *K*-fluorescence emission processes were considered: *K-L2*, *K-L3*, *K-L-M2*, *K-M3*, *K-N2*, *K-N3*, and *K-X* radiative transitions and the *K-L-X* Auger transitions,<sup>54</sup> where *X* denotes a shell with negligible binding energy. The initial x-ray photon was assumed to be locally absorbed when (a) the x-ray photon energy was higher than the *K*-shell binding energy  $U_K$  and at the same time the photoelectric effect occurred in the *L*-shell, (b) the x-ray photon energy was higher than the average *L*-shell binding energy  $U_L$  (Ref.

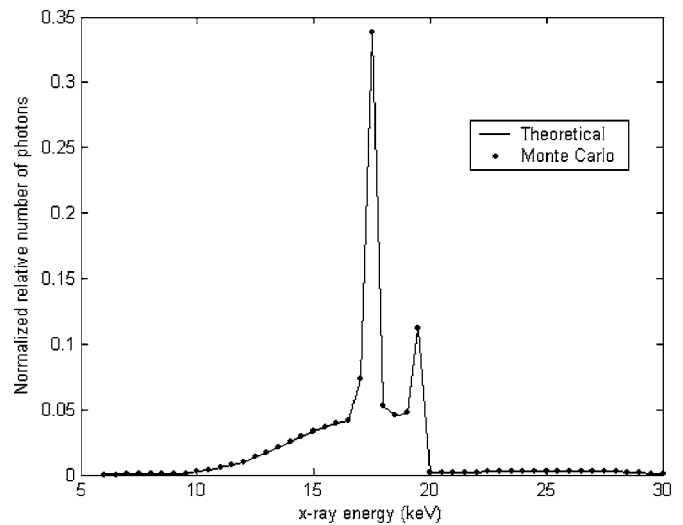


Fig. 2. Comparison of Monte Carlo samples (dots) and the theoretical distribution of a 30 kVp Mo x-ray spectrum filtered by 0.051 mm Mo.

54) and lower than the *K*-shell binding energy  $U_K$ , and (c) the x-ray photon energy was lower than 5 keV (cutoff energy<sup>18</sup>).

If the x-ray photon undergoes a scattering process, the direction of the scattered photon is derived by sampling the corresponding polar angle  $\theta$  and azimuthal angle  $\phi$  of the scattering process. The polar angle  $\theta$  is sampled randomly from the differential cross section using the sampling algorithm, described by Chan and Doi<sup>21</sup> and Brusa *et al.*,<sup>55</sup> for coherent and incoherent scattering, respectively. In both aforementioned types of scatter, the azimuthal angle  $\phi$  of the scattered photon is sampled randomly in the interval  $[0, 2\pi)$ . When an incoherent scattering event takes place, the energy difference between the incident and the scattered photon goes to the loosely bound atomic electron (recoil electron) as kinetic energy, considering that the electron had negligible binding energy. In this study, the recoil electron was assumed to be locally absorbed.

All sampling procedures were verified by comparing results obtained by the Monte Carlo simulation against results derived analytically using the theoretical probability density functions. The average relative difference between the Monte Carlo simulation and the theoretically obtained values was found to be (a) 1.8% for the sampling of the x-ray spectrum (Fig. 2), (b) 0.6% for the sampling of the fpl (Fig. 3), (c) 2.4% for sampling the polar angle  $\theta$  in coherent scattering (Fig. 4), and (d) 2.1% for sampling the polar angle  $\theta$  in incoherent scattering (Fig. 5).

## D. Light production

After an x-ray interaction event, contributing to energy deposition within the phosphor material, light photons are created following an isotropic distribution. The number  $G$  of these light photons is given as follows:<sup>14</sup>

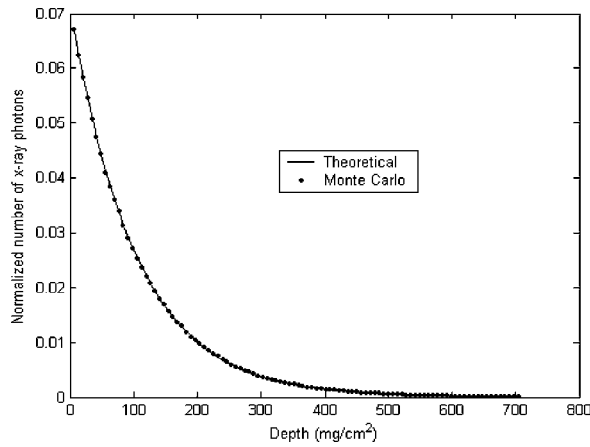


FIG. 3. Comparison of  $10^6$  Monte Carlo samples (dots) and the theoretical curve of free path length for a 60 keV monochromatic x-ray beam in  $\text{Gd}_2\text{O}_2\text{S:Tb}$  phosphor screen.

$$\bar{G}(E) = \eta_c \frac{E}{E_\lambda}, \quad (1)$$

where  $E$  is the absorbed energy of the x-ray photon,  $\eta_c$  is the intrinsic x-ray to light conversion efficiency<sup>56</sup> of the phosphor, and  $E_\lambda$  is the mean energy of the light photons created within the phosphor mass. Mean energy was employed in relation (1) instead of the whole light spectrum. We used the value  $E_\lambda = 2.4 \times 10^{-3}$  keV, which corresponds to the mean light photon energy of the  $\text{Gd}_2\text{O}_2\text{S:Tb}$  phosphor.<sup>14</sup> The simulation of the light spectrum is quite complicated because of the statistical uncertainties arising from (a) the electron transition probabilities in the low energy atomic levels<sup>54</sup> and (b) the effects of the activator on these levels.<sup>56,57</sup> It has been previously shown that the statistical fluctuations of the x-ray to light conversion process follow a probability distribution, which has not been expressed analytically. However, it may be approximated using experimental data.<sup>58,59</sup> The excess of this distribution function over a Poisson distribution has been expressed<sup>58</sup> by the Poisson excess noise ( $\varepsilon$ ) given as follows:

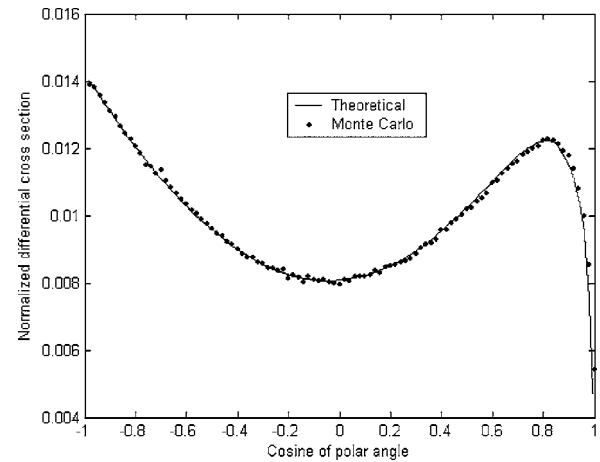


FIG. 5. Comparison of  $10^6$  Monte Carlo samples (dots) and the theoretical curve of polar angle distribution for incoherent scattering of a 60 keV monochromatic x-ray beam in Gd element.

$$\varepsilon = \left( \frac{\sigma_{G(E)}^2}{\bar{G}(E)} \right) - 1, \quad (2)$$

where  $\bar{G}(E)$  is the average number of light photons produced per absorbed x-ray photon and  $\sigma_{G(E)}^2$  is the variance of the probability distribution. In the present study, the Swank factor<sup>29</sup> as well as the DQE values were predicted by sampling the number of produced light photons, using the particular probability distribution, and by determining the corresponding statistical moments ( $m_i$ ) of the light distribution detected by the optical detector, as described in previous studies.<sup>8–10</sup>

## E. Light transport

Just after their creation, light photons are transmitted through the screen material towards the screen surfaces. During transmission, light suffers attenuation mainly caused by the presence of the phosphor grains. Since the geometry of our model implies a homogeneous distribution of phosphor grains, Mie theory<sup>42</sup> can be applied to describe adequately the light extinction within a phosphor screen (see Appendix A). At the site of light photon interaction, the type of interaction may be determined by the relative probabilities of light absorption and light scattering effects. The probability of light absorption  $P_{abs}$  is defined as follows:

$$P_{abs} = m_{abs} / (m_{abs} + m_{sct}), \quad (3)$$

where  $m_{abs}$ ,  $m_{sct}$  correspond to light absorption and light scattering coefficients, respectively. The azimuthal angle  $\phi$  of the scattered photon was sampled randomly in  $[0, 2\pi)$ . The polar angle  $\theta$  was sampled from the Henyey-Greenstein<sup>60,61</sup> (see Appendix B) probability density function, which is a good approximation of the phase function for light photons scattered according to Mie theory. The sampling procedure can be verified by comparing results obtained by Monte Carlo simulation with the theoretical polar angular distribution, as shown in Fig. 6. Assuming grain diameter equal to  $7 \mu\text{m}$  for

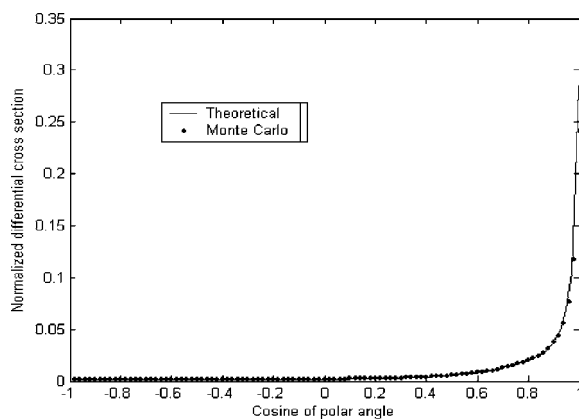


FIG. 4. Comparison of  $10^6$  Monte Carlo samples (dots) and the theoretical curve of polar angle distribution for coherent scattering of a 60 keV monochromatic x-ray beam in Gd element.

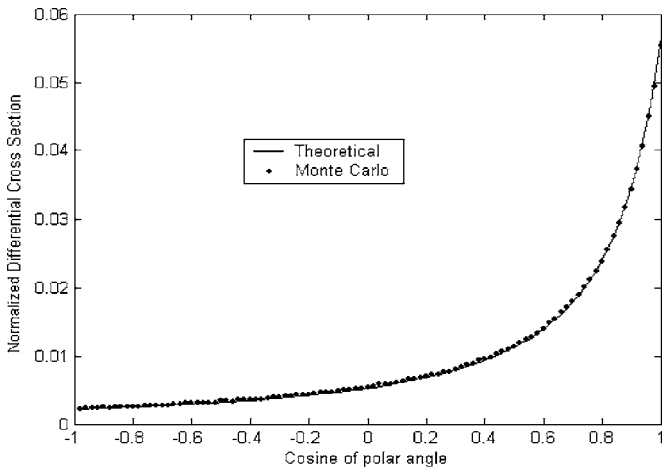


FIG. 6. Comparison of  $10^6$  Monte Carlo samples (dots) and the Henyey-Greenstein theoretical distribution of polar angle distribution for  $\text{Gd}_2\text{O}_2\text{S}:\text{Tb}$  phosphor screen with grain size  $7 \mu\text{m}$ .

$\text{Gd}_2\text{O}_2\text{S}:\text{Tb}$  phosphor material (anisotropy factor  $g=0.494$ , see Appendix B), the average relative difference between Monte Carlo and theoretical values was found 1.2%.

As described above, light propagation was simulated via Mie theory. Applying Mie calculations, light absorption and light scattering coefficients,  $m_{abs}, m_{sct}$ , are related to the absorption,  $Q_{abs}$ , and the scattering,  $Q_{sct}$ , efficiency factors<sup>41,42,62</sup> and to the complex elements,  $S_1(\theta)$  and  $S_2(\theta)$ , of the scattering matrix.<sup>41,42,62</sup> These quantities were correctly simulated according to the validation that is shown in Table I (see Appendix A). The comparison was carried out for data relative to the numerical values, which correspond to the complex refractive index of phosphor materials (complex refractive index of  $\text{Gd}_2\text{O}_2\text{S}:\text{Tb}$ :  $2.3-10^{-6}i$ , where 2.3 and  $10^{-6}$  represent the real and the imaginary parts, respectively). For the  $\text{Gd}_2\text{O}_2\text{S}:\text{Tb}$  phosphor material, Moy<sup>52</sup> has reported a refractive index value of higher than 2. Radcliffe *et al.*<sup>37</sup> have used a value of 2.4 in combination with a value of 1.4 for the refractive index of the binder, both of which gave a reasonable fit to experimental data. In the present study, the real part of the complex refractive index of  $\text{Gd}_2\text{O}_2\text{S}:\text{Tb}$  was taken equal to 2.3 using binder's refractive index<sup>33</sup> equal to 1.353. Following previous studies,<sup>36,41</sup> the imaginary part was assumed to be of the order of  $10^{-6}$ , for wavelengths within the visible region.

## F. Reflection at the boundaries

During a light photon trajectory, when the light photon hits one of the phosphor screen boundaries, it may either escape or internally be reflected. If we consider that  $z_0$  and  $z_1$

are the corresponding  $z$  coordinates of the front and rear side boundaries of phosphor screen, the trajectory of light photon may be indicated according to the following procedure:

- (i) The distance  $d_1$  between the last light photon interaction site and the boundary is calculated:

$$d_1 = \begin{cases} (z - z_0)/(-\cos \theta), & \text{for } \cos \theta < 0, \\ (z_1 - z)/\cos \theta, & \text{for } \cos \theta > 0, \end{cases} \quad (4)$$

- (ii) The angle of incidence  $\theta$  is evaluated and, with the help of Snell's law, the angle of transmission  $\omega$  is calculated as a function of  $\theta$ , of the relative complex refractive index of the phosphor screen  $m_i$  (phosphor material), and of the refractive index of the transmitting medium  $m_t$  (air, film, or photosensitive material), as follows:

$$\theta = \cos^{-1}(|\cos \theta|) \quad \text{and} \quad \omega = \sin^{-1}\left(\frac{m_i}{m_t} \sin \theta\right). \quad (5)$$

- (iii) The probability of the average light photon specular reflectance can be calculated from Fresnel's formulas<sup>41,63</sup> multiplied by a factor  $S_C$  correcting for the roughness of the screen's surface, given by the following equation.<sup>63,64</sup>

$$S_C = \exp\left[-\left(\frac{2\sqrt{2}\pi n \delta}{\lambda}\right)^2\right], \quad (6)$$

where  $\delta$  is the root mean square (rms) roughness expressing surface irregularities,  $\lambda$  is the light wavelength, and  $n$  is the real part of the refractive index of the transmitting medium. Values of  $S_C$  near to unity imply interfaces of high surface smoothness. For example, assuming  $\delta=3 \text{ nm}$ ,  $n=1.5$ , and  $\lambda=545 \text{ nm}$ , Eq. (6) results in a factor  $S_C$  equal to 0.988, implying a slight reduction in specular reflectance. Therefore, surface irregularities may cause (a) a slight reduction in specular reflectance and (b) the presence of diffuse reflectance. In the latter case, light photons are reflected in random directions. In the present study, light specular reflectance was simulated assuming smooth boundary surface and, thus, the effect of diffuse reflectance was not taken into consideration.

- (iv) The light photon is internally reflected, otherwise it escapes the phosphor screen. In case of reflection, the light photon transportation is described as follows:<sup>65</sup>

- (a) A new direction is calculated by transforming the direction cosines to  $(a, b, c) = (\sin \theta \cos \phi, \sin \theta \sin \phi, -\cos \theta)$ .

TABLE I. Comparison of  $Q_{ext}$ ,  $Q_{sca}$ ,  $S_1(0)$ ,  $S_2(0)$ ,  $S_1(\pi)$ , and  $S_2(\pi)$  between Hong Du's<sup>62</sup> 2004 calculations and those obtained from our study.

	$M$	$X$	$Q_{ext}$	$Q_{sca}$	$S_1(0)=S_2(0)$	$S_1(\pi)=-S_2(\pi)$
Present study	$1.33-10^{-5}i$	100	2.101 32	2.096 59	5253-24.319i	-56.5921+484.251i
Hong Du <sup>62</sup>	$1.33-10^{-5}i$	100	2.101 32	2.096 59	5253-24.319i	-56.5921+484.251i

- (b) The light photon propagates within phosphor material having a new free path length equal to  $fpl-d_1$ .

### G. Output parameters

Employing the previously described simulation, numerical evaluations concerning the x-ray and light photon absorption or escape events were carried out. Additionally, for every x-ray interaction and absorption event, information on the deposited amount of the x-ray energy, as well information on the spatial distribution of the emitted light, was obtained. These evaluations and the corresponding information were used in the evaluation of the following phosphor screen parameters and imaging characteristics:

- (i) The quantum detection efficiency (QDE) corresponding to the number of absorbed x-ray photons with respect to the incident x-ray photons.
- (ii) The energy absorption efficiency (EAE) corresponding to the absorbed energy of primary radiation with respect to the incident x-ray energy.
- (iii) The number of emitted light photons per incident x-ray photon.
- (iv) The point spread function (PSF): the two-dimensional spatial position of light photons along screen length.
- (v) The modulation transfer function (MTF): the discrete Fourier transform (DFT) of the line-spread function (LSF), which was obtained by integrating the PSF over one axis.
- (vi) The detective quantum efficiency (DQE) expressed by the Swank factor (SF) multiplied by the quantum detection efficiency (QDE). The Swank factor was obtained by evaluating the corresponding statistical moments ( $m_i$ ) of the light distribution detected by the optical detector.

Applying  $10^4$  monoenergetic x-ray photons of 18 keV ( $9 \times 10^6$  light photon histories) for  $Gd_2O_2S:Tb$  phosphor material (thickness:  $31.7 \text{ mg/cm}^2$ , grain size:  $7 \text{ }\mu\text{m}$ , packing density: 50%), approximately 14 h of computation time are required using a single-processor P4 with 3.00 GHz and 512 Mbyte access memory.

### III. RESULTS

The quantum detection efficiency of  $Gd_2O_2S:Tb$  phosphor with respect to the incident x-ray energy is shown in Fig. 7. In this figure Monte Carlo results are compared with experimental data obtained by Dick and Motz,<sup>9</sup> for energies ranging from 18 to 69 keV. The curves correspond to  $31.7 \text{ mg/cm}^2$  screen coating weight,  $7 \text{ }\mu\text{m}$  mean grain size, and 50% packing density.<sup>4,14</sup> QDE was evaluated by considering parallel, 3 mm thick, monoenergetic x-ray beams. In this evaluation, the number of reabsorbed  $K$  x-ray photons for energies above the  $K$ -edge of the Gd element was also taken into account. All curves correspond to data obtained behind the non-irradiated screen surface. This configuration is often referred to as front screen configuration or transmission mode and corresponds to the screen-optical detector

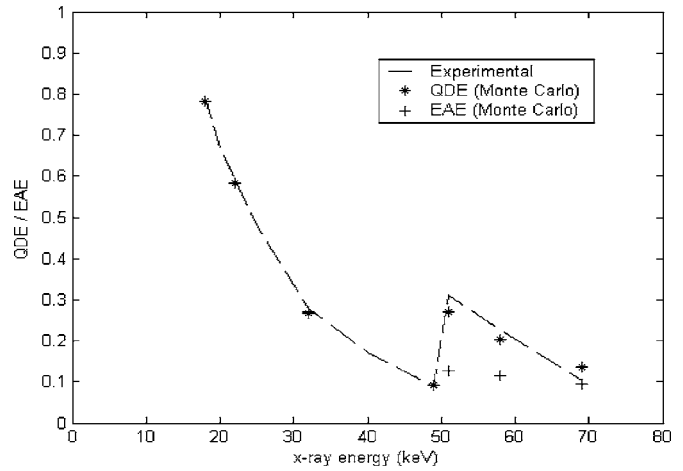


FIG. 7. The variation of QDE and EAE as a function of the incident x-ray energy. Comparison between Monte Carlo values (dots) and experimental (QDE) measurements<sup>9</sup> for  $Gd_2O_2S:Tb$  phosphor material (thickness:  $31.7 \text{ mg/cm}^2$ , packing density: 50%, grain size:  $7 \text{ }\mu\text{m}$ ).

combination incorporated in digital imaging detectors. Results for the energy absorption efficiency (EAE), obtained under similar conditions, are also given in the same graph. Both QDE and EAE were estimated with a statistical error less than 0.1%.

QDE and EAE were found almost identical in the energy range from 18 to 25 keV. Above 25 keV, the values of EAE were found slightly higher than QDE. This difference was due to the increasing number of scattering events (inelastic scattering) occurring for energies higher than 25 keV. Even if scattered photons escape the screen, and are thus not accounted for in the calculation of QDE, a small fraction of energy is still deposited within the phosphor. This small fraction increases slightly the values of EAE with respect to those of QDE. Above 50.2 keV, a  $K$ -fluorescence photon is generated that may escape the phosphor screen, even though the incident x-ray photon is totally absorbed. The energy conveyed by the  $K$ -fluorescence photon is considerably higher than the energy locally deposited by the incident photon. As a result, QDE values, expressing the fraction of absorbed incident x-ray photons, are significantly higher than those of EAE, expressing the fraction of locally absorbed energy.

Table II shows the number of light photons emitted by the non-irradiated screen surface (transmission mode or front screen configuration) per absorbed x-ray photon for various x-ray photon energies from 18 to 69 keV. Monte Carlo results are compared with experimental data from the work by Dick and Motz.<sup>9</sup> These data were obtained under experimental irradiation conditions similar to those simulated in our method. In the evaluation of light photons per absorbed x-ray photon, the light reflection at the screen-substrate<sup>28</sup> interface was also taken into account (see Sec. II F). The average value of light reflectance  $R(\theta)$ , for all possible incident angles at the screen-substrate interface, was found approximately equal to 0.30 (fraction of escaped light photons 70%). This value was obtained using the following data for the

TABLE II. Comparison of the number of emitted light photons per absorbed x ray between Dick and Motz;<sup>9</sup> 1981 experimental measurements and those obtained in our study for various incident x-ray energies.

Incident energy (keV)	Gd <sub>2</sub> O <sub>2</sub> S:Tb (thickness 31.7 mg/cm <sup>2</sup> )						
	18	22	32	49	51	58	69
	No. of emitted light photons per absorbed x-ray						
Dick and Motz <sup>9</sup>	365±73	470±94	645±129	945±189	700±140	785±157	890±178
Present study	356±3	463±4	695±12	1089±43	710±8	924±25	1282±37

relative complex refractive index:  $m_{material} = n_{grain}/n_{medium} = 2.3/1.353 = 1.7$  and  $m_t = 1.52$ , where  $m_{material}$  is the relative complex refractive index of the phosphor screen [ $m_i$  in Eq. (5)],  $n_{grain}$  is the refractive index of the phosphor material (Gd<sub>2</sub>O<sub>2</sub>S:Tb),  $n_{medium}$  is the refractive index of the binder material (Na<sub>2</sub>SiO<sub>3</sub>),<sup>53</sup> and  $m_t$  is the refractive index of the transmitting medium  $m_t$  (glass).

Apart from the data obtained at 69 keV, our Monte Carlo simulation results are in adequate agreement with the results from experimental measurements. Deviations from full coincidence may be reasonable if we consider (a) the estimated uncertainty in experimental data,<sup>8</sup> which is of the order of 20%, (b) the possible count loss during experimental measurements,<sup>8</sup> which is 3%, (c) the error, in our model, arising from the assumption of monochromatic light photons,<sup>14</sup> (d) the statistical error in coefficients taken from data bases,<sup>47,48</sup> (e) the systematic error arising from our assumption of 50% packing density, 7 μm grain size, and 0.15 intrinsic efficiency, and (f) the statistical error that arise from Monte Carlo simulations.

Table III shows data obtained by the Monte Carlo model corresponding to the fraction of emitted light (in transmission mode) with respect to the light produced within the phosphor, as well as with respect to the contribution of various energy deposition processes to the emitted light. The

energy deposition processes considered were the following: (a) x-ray photons absorption without undergoing any scatter event, (b) x-ray photons absorption, after, at least, one scatter event, (c) *K*-characteristic photons absorption, (d) energy deposition by Auger electrons produced in the *K*-shell, and (e) energy deposition by electrons released during inelastic scattering. All data provided correspond to Gd<sub>2</sub>O<sub>2</sub>S:Tb phosphor (thickness: 31 mg/cm<sup>2</sup>, grain size: 7 μm, packing density: 50%), in the energy range from 18 keV up to 69 keV.

Figure 8 illustrates a comparison between an experimentally determined<sup>14</sup> and a Monte Carlo simulated modulation transfer function (MTF) of a Gd<sub>2</sub>O<sub>2</sub>S:Tb screen (thickness: 31.7 mg/cm<sup>2</sup>, grain size: 7 μm, packing density: 50%). Both curves correspond to similar irradiation conditions: 30 kVp poly-energetic molybdenum x-ray spectrum, filtered by 0.051 mm of molybdenum and 4.2 cm of Lucite to simulate beam hardening by an average breast. Additionally, narrow beam geometry at the centre of phosphor screen surface was assumed.<sup>14</sup> As it can be observed in Fig. 8, there is a high degree of coincidence between the experimental and the Monte Carlo predicted MTF values. In fact, it was calculated that the absolute value of the average relative difference between the two curves at all spatial frequencies was 1%. The latter resulted from the slightly higher Monte Carlo simu-

TABLE III. Light emitted per light produced of Gd<sub>2</sub>O<sub>2</sub>S:Tb (thickness 31.7 mg/cm<sup>2</sup>) for various incident x-ray energies. Contribution of each physical process to the emitted light (transmission mode).

Incident energy (keV)	Gd <sub>2</sub> O <sub>2</sub> S:Tb (thickness 31.7 mg/cm <sup>2</sup> )			
	18	49	51	69
Light emitted per light produced % (Front screen)	42.41±0.16	48.64±0.69	47.35±0.29	47.94±0.43
Contribution to light emitted (Front screen configuration)				
Local deposition of the initial photon % (without scatter event)	97.46±0.19	97.82±0.5	62.82±1.01	78.26±0.62
Local deposition of the initial photon % (with scatter event)	2.53±0.19	1.83±0.48	0.81±0.23	0.78±0.16
<i>K</i> -characteristic radiation %			25.96±0.46	14.91±1.02
<i>K</i> -auger electrons %			10.26±0.74	5.67±0.64
Compton electrons %	0.0057±0.0022	0.34±0.08	0.15±0.02	0.36±0.05

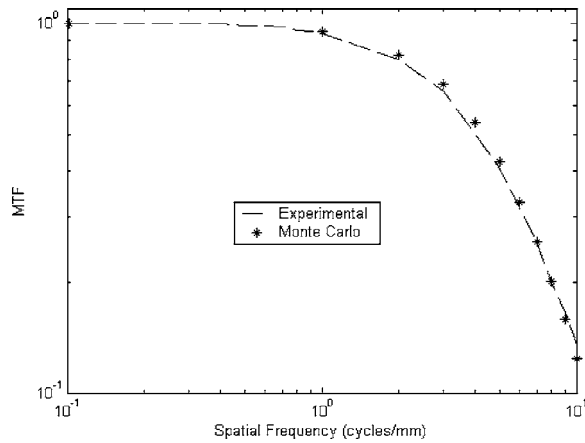


FIG. 8. The variation of MTF as a function of spatial frequency. Comparison between Monte Carlo values (dots) and experimental measurements<sup>14</sup> for  $\text{Gd}_2\text{O}_2\text{S:Tb}$  phosphor material (thickness:  $31.7 \text{ mg/cm}^2$ , packing density: 50%, grain size:  $7 \mu\text{m}$ , x-ray tube voltage: 30 kVp, filter: 0.0051 mm Mo, 4.2 cm Lucite).

lated values. This systematic error may probably have arisen from our assumption of constant grain size [equal to the alleged by the manufacturer ( $7 \mu\text{m}$ )]. If this is not the case, then a deviation from the experimental MTF may be expected, due to variations in packing density (or grain spatial distribution) and in grain size. In the present study, the MTF of the film was taken to be unity.<sup>58,66</sup>

To investigate the effect of grain size and packing density on MTF, Monte Carlo results, shown in Figs. 9 and 10, were obtained. As it can be observed, both grain size and packing density affect significantly MTF values. Higher MTF corresponds to small grain size (Fig. 9) and high packing density (Fig. 10). The effect of grain size and packing density may be explained by considering that the increased number of grains, either in a small sized grain distribution or in a denser distribution, increases the number of light scattering events.

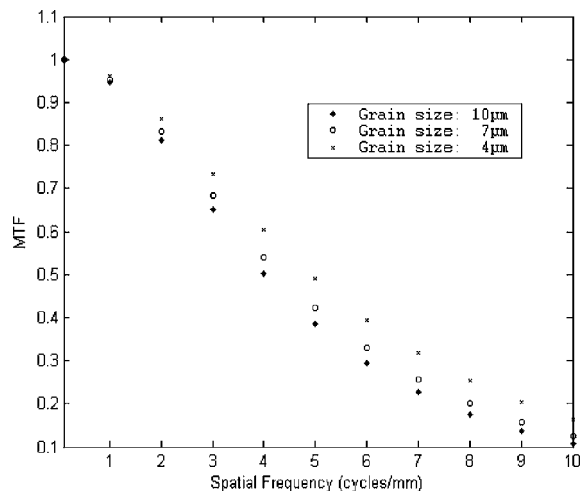


FIG. 9. The variation of MTF as a function of spatial frequency for three different values of grain size (4, 7, and  $10 \mu\text{m}$ ) for  $\text{Gd}_2\text{O}_2\text{S:Tb}$  phosphor material (thickness:  $31.7 \text{ mg/cm}^2$ , packing density: 50%, x-ray tube voltage: 30 kVp, filter: 0.0051 mm Mo, 4.2 cm Lucite).

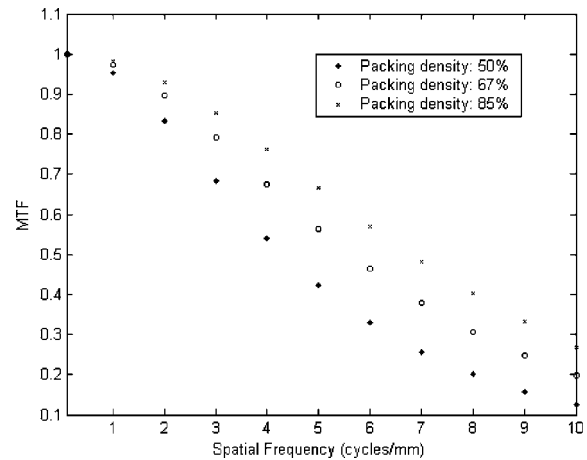


FIG. 10. The variation of MTF as a function of spatial frequency for three different values of packing density (50%, 67%, 85%) for  $\text{Gd}_2\text{O}_2\text{S:Tb}$  phosphor material (thickness:  $31.7 \text{ mg/cm}^2$ , grain size:  $7 \mu\text{m}$ , x-ray tube voltage: 30 kVp, filter: 0.0051 mm Mo, 4.2 cm Lucite).

In that case, laterally directed light photons, which follow large distances to escape the screen, undergo a larger number of interactions. Therefore, the probability of lateral photon extinction increases. Thus, the total amount of light propagates to the screen output following a spatial distribution of higher forward directivity, resulting in better MTF values.<sup>30</sup>

Table IV gives the DQE values with respect to x-ray energy. Monte Carlo values are compared with experimental data, obtained by Dick and Motz<sup>9</sup> for energies ranging from 18 to 69 keV. Up to the energy of  $K$ -absorption edge, DQE values were estimated assuming a Poisson distribution. [i.e.,  $\varepsilon=0$ , see Eq. (2)]. For x-ray energies above the  $K$ -edge, DQE values were predicted by (a) taking into account the QDE values obtained by the detected incident x-ray photons<sup>8-10</sup> and (b) evaluating the Swank factor, assuming a Poisson distribution at 51 and 58 keV, and a non-Poisson distribution at 69 keV, considering  $\varepsilon/\bar{G}(E)=0.3$  [see Eq. (2)]. DQE values were found to be in excellent agreement with the experimental data.

#### IV. DISCUSSION

The light interactions within phosphor materials has been previously described in terms of optical parameters incorporated in analytical models published by Hamaker, Ludwig, and Swank.<sup>26-29</sup> These models have been developed either by assuming one-dimensional light propagation or by using suitable approximations to the photon diffusion equation. The values of the optical parameters have been obtained by fitting model equations to experimental data. However, it has been observed that these values were, more or less, affected by the thickness of the phosphor. This was attributed to the limitations of the aforementioned models to accurately express phosphor inhomogeneities arising from the granular structure of the screens. The optical coefficients related to these models have been also used in Monte Carlo studies<sup>36</sup> to simulate light interactions within phosphor screens. Badano *et al.*<sup>39</sup> developed a model using the DETECT II simulation

TABLE IV. Comparison of DQE values between Dick and Motz's<sup>9</sup> 1981 experimental measurements and those obtained in our study for various incident x-ray energies.

Gd <sub>2</sub> O <sub>2</sub> S:Tb Phosphor thickness: 31.7 mg/cm <sup>2</sup>							
Incident energy (keV)	18	22	32	49	51	58	69
	Detective quantum efficiency (DQE)						
Dick and Motz <sup>a</sup>	0.58	0.44	0.19	0.07	0.18	0.14	0.07
Present study	0.57	0.43	0.20	0.07	0.16	0.14	0.07

code and provided a better fit to experimental data. In the present study, the material's complex refractive index was used as an input optical parameter. Following previous studies,<sup>36,41,42,62</sup> it was considered that in a phosphor material the real part of the refractive index indicates light scattering, and the imaginary part indicates light absorption. It was also assumed that the imaginary part of the material's complex refractive index is not negligible. Using refractive index data and applying Mie scattering theory in our calculations, microscopic probabilities were used to simulate light transport within the phosphor material. Based on such considerations, we have developed our model in such a way that, apart from the complex refractive index, the only optical data required to express screen properties and their effect on image characteristics were the values of the intrinsic conversion efficiency and the light wavelength. Within this treatment, the relative probability of light absorption, with respect to light scattering, depends on the size of phosphor grains and on the wavelength of the transmitted light. At the phosphor screen output, the fraction of escaping light photons was related to the number of light interaction events taking place within the phosphor material. For a given grain size and packing density, this number was also associated to the corresponding phosphor screen thickness. It has been previously estimated that analytical models, based on diffusion equation, cannot accurately describe the performance of thin screens and corresponding results are of limited accuracy.<sup>32</sup> The present study attempts to overcome these limitations. The light spatial distribution at screen output can be predicted and information of phosphor screen performance for different virtual experimental setups can be extracted. As it may be observed from Fig. 7, the values predicted for the QDE show slight deviations with respect to experimental data. These deviations appear more clearly at energies above the *K*-edge. At these energies, both experimental data and our Monte Carlo results are affected by the presence of the *K*-characteristic radiation. In order to investigate this effect, the simulation of *K*-characteristic radiation was examined by comparing the fraction of escaped *K*-photons, as predicted by our code, with previous calculations.<sup>11</sup> As it is shown in Table V, both data were found to be in excellent agreement. Hence, the deviations may be probably due either to experimental uncertainties or to uncertainties in the attenuation coefficients values above the *K*-edge of published data.<sup>46</sup> In addition, attenuation coefficient uncertainties, which have been also discussed

by Chan and Doi,<sup>21</sup> may also be responsible for deviations in the prediction of emitted light photons per absorbed x ray, especially at 69 keV (see Table II).

To further investigate this issue, e.g., the influence of the x-ray coefficient uncertainties on the accurate determination of the emitted light, we tried to show that light is attenuated in the same manner independently from the input value of the incident x-ray energy (e.g., 51, 58, and 69 keV). In this case, we may expect equal portions of the generated light photons to escape the phosphor (from the both sides: irradiated and non-irradiated) for different values of incident x-ray energy. This would imply that the total number of the emitted light photons, or the total light energy fluence emitted by the screen, is proportional to the number of light photons generated within the phosphor, which in turn is proportional to the total amount of x-ray energy deposited. Hence, in order to test the aforementioned consideration, the ratio of the total light energy fluence emitted by both screen surfaces (both the irradiated and the non-irradiated sides) over the total amount of energy absorbed was examined. This ratio was evaluated for various incident x-ray photon energies. More specifically, by applying x-ray beams with corresponding energies 51, 58, and 69 keV, the above ratio was found equal to 0.1492. This invariable value of the ratio, which equals the intrinsic efficiency ( $n_c=0.15$ ) minus the fraction of light energy flux absorbed in the phosphor, indicates that light losses are similar for all x-ray energy values. Therefore, variations in the amount of the emitted light in each phosphor screen side are due to the absorbed energy depth distribution at the corresponding incident x-ray energy. Taking into account that for each 1 keV x-ray energy deposition, 62 light photons are produced, small deviations in the energy depth of the absorbed x-rays could cause quite large deviations in the

TABLE V. Comparison of the escaped *K*-photons fraction between Venema's<sup>11</sup> 1979 calculations and these obtained from our study.

Gd <sub>2</sub> O <sub>2</sub> S:Tb (thickness 105 mg/cm <sup>2</sup> )			
Incident energy (keV)	51	58	69
	Fraction of escaped <i>K</i> -photons		
Present study	60.45% ± 0.24	60.52% ± 0.25	60.21% ± 0.29
Venema <sup>11</sup>	60%		

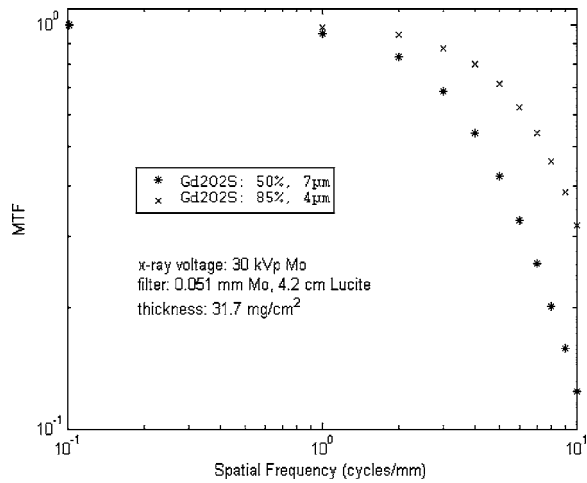


FIG. 11. The variation of MTF as a function of spatial frequency. Comparison between the conventional  $\text{Gd}_2\text{O}_2\text{S:Tb}$  screen (packing density 50%, grain size  $7\ \mu\text{m}$ ) and the high packing density, small grain size  $\text{Gd}_2\text{O}_2\text{S:Tb}$  screen (packing density 85% and grain size  $4\ \mu\text{m}$ ) with coating weight  $31.7\ \text{mg}/\text{cm}^2$ .

amount of light emitted by each screen surface. Actually, according to Nishikawa and Yaffe's model,<sup>14</sup> for phosphor screens of equal thickness, each variation on the amount of light that escapes to the screen output is due to the depth of each x-ray interaction and the corresponding amount of the deposited energy on it.

According to MTF data shown in Figs. 9 and 10, the size of the phosphor grains and their spatial distribution (packing density) affect significantly the MTF values, which improve with decreasing grain size and with increasing packing density. It has been previously shown that screen packing density may remain invariant when the size of the grains varies.<sup>31</sup> However, Blasse and Grabmaier<sup>4</sup> suggested that apart from obtaining the desired particle size, powder materials with a reduced porosity (higher packing density) can be synthesized. This may be achieved using a sintering process at elevated temperature to produce phosphor layers in ceramic form. In such a case, the increased fraction of grains within phosphor screen increases the number of light scattering events. Under Mie scattering conditions, this increases the overall directivity of the light flux propagation within the screen mass and may affect the spatial distribution of the light at the screen emitting surface, resulting in a significantly better MTF. The significance of this issue was verified by comparing a conventional  $\text{Gd}_2\text{O}_2\text{S:Tb}$  screen (packing density: 50%, grain size:  $7\ \mu\text{m}$ ) with a nonconventional  $\text{Gd}_2\text{O}_2\text{S:Tb}$  screen (packing density: 85%, grain size:  $4\ \mu\text{m}$ ) of equal coating weight ( $31.7\ \text{mg}/\text{cm}^2$ ). Comparison was performed by applying a 30 kVp poly-energetic molybdenum x-ray spectrum, filtered by 0.051 mm of molybdenum and 4.2 cm of Lucite. As shown in Fig. 11, by selecting a phosphor grain size of  $4\ \mu\text{m}$  and a packing density of 85%, a  $\text{Gd}_2\text{O}_2\text{S:Tb}$  screen may exhibit considerably higher MTF.

Similar results were observed by comparing MTF data, assuming equal screen thickness ( $85\ \mu\text{m}$ ). In Fig. 12 are shown MTF curves indicating the superiority of the high

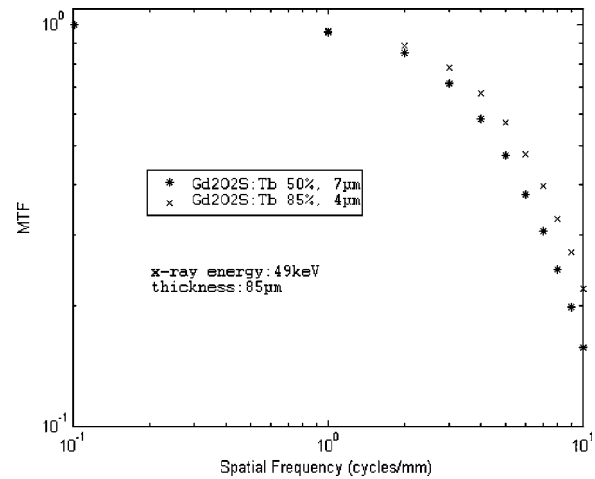


FIG. 12. The variation of MTF as a function of spatial frequency. Comparison between the conventional  $\text{Gd}_2\text{O}_2\text{S:Tb}$  screen (packing density 50%, grain size  $7\ \mu\text{m}$ ) and the high packing density, small grain size  $\text{Gd}_2\text{O}_2\text{S:Tb}$  screen (packing density 85% and grain size  $4\ \mu\text{m}$ ) with thickness  $85\ \mu\text{m}$ .

packing density, small grain size  $\text{Gd}_2\text{O}_2\text{S}$  screen over the conventional  $\text{Gd}_2\text{O}_2\text{S}$  screens. In order to examine the light emission efficiency under similar conditions, results of light emitted photons per incident x ray are also shown in Table VI. Results were obtained for the conventional  $\text{Gd}_2\text{O}_2\text{S:Tb}$  screen (packing density: 50%, grain size:  $7\ \mu\text{m}$ ) as well as for the high packing density, small grain  $\text{Gd}_2\text{O}_2\text{S:Tb}$  screen (packing density: 85%, grain size:  $4\ \mu\text{m}$ ). As it may be seen (e.g., at 49 keV x-ray energy), in addition to better resolution properties, the high packing density, small grain size  $\text{Gd}_2\text{O}_2\text{S:Tb}$  screen also exhibits better light emission properties.

An  $85\ \mu\text{m}$  thick  $\text{Gd}_2\text{O}_2\text{S}$  phosphor layer with 50% packing density corresponds to coating weight of  $31.7\ \text{mg}/\text{cm}^2$ . For 85% packing density, the corresponding coating weight is  $53\ \text{mg}/\text{cm}^2$ . This increases x-ray absorption and, therefore, the amount of light, initially created within the screen, is higher. However, light attenuation, determined by the number of light-phosphor grain interactions per unit of length, increases with packing density. Thus, light absorbed per light produced is higher, being approximately 5% in the case of  $\text{Gd}_2\text{O}_2\text{S:Tb}$  (85%,  $4\ \mu\text{m}$ ) instead of 0.5% in the case of  $\text{Gd}_2\text{O}_2\text{S:Tb}$  (50%,  $7\ \mu\text{m}$ ). In conclusion, by increasing

TABLE VI. Comparison of light emitted per incident x ray between the conventional  $\text{Gd}_2\text{O}_2\text{S:Tb}$  screen (packing density 50%, grain size  $7\ \mu\text{m}$ ) and the high packing density, small grain size  $\text{Gd}_2\text{O}_2\text{S:Tb}$  screen (packing density 85% and grain size  $4\ \mu\text{m}$ ).

	$\text{Gd}_2\text{O}_2\text{S:Tb}$ Phosphor thickness: $85\ \mu\text{m}$			
	18	49	51	69
Incident energy (keV)				
	Light emitted per incident x ray (Front screen)			
Grain size: $7\ \mu\text{m}$	$275 \pm 2$	$101 \pm 5$	$192 \pm 3$	$173 \pm 5$
Packing density: 50%				
Grain size: $4\ \mu\text{m}$	$244 \pm 3$	$143 \pm 5$	$294 \pm 6$	$264 \pm 7$
Packing density: 85%				

the packing density of a screen, the resolution (MTF) as well as the light emission properties become better. This may provide an advantage over techniques based on absorbing dyes incorporation for screen resolution improvement.

## V. CONCLUSIONS

A new computational model, based on Monte Carlo methods, has been developed to simulate the x-ray and light interaction mechanisms within granular phosphor screens. The model was validated with published experimental data and was used to perform the x-ray absorption and the light emission properties of powder screens in relation to x-ray energy. The model, by using the physical characteristics (complex refractive index, light wavelength) of the phosphor materials, applied Mie theory in order to describe light propagation. The effect of the material structure parameters (grain size, packing density) on light spread, as well as on MTF, was investigated. It was shown that these parameters were of crucial importance and can affect the number of light interactions, the angle of the scattered light (the anisotropy factor), and therefore the spatial resolution performance of phosphor screens. Granular screens of higher packing density and lower grain size were found to present considerably better light emission (approximately 1.5 times higher amount of emitted light) and spatial resolution properties (approximately MTF=0.22 instead of MTF=0.16 at 10 cycles/mm) in comparison with conventional screens, under similar conditions (e.g., equal x-ray energy and phosphor thickness).

## ACKNOWLEDGMENTS

This work was financially supported by the Greek Ministry of Education (through EPEAEK ‘‘Archimidis I’’).

## APPENDIX A: MIE THEORY

Light absorption and scattering coefficients  $m_{abs}, m_{sct}$  are given by the following equations:

$$m_{abs} = V_d A Q_{abs} \quad \text{and} \quad m_{sct} = V_d A Q_{sct}, \quad (\text{A1})$$

where each coefficient depends on the volume density of phosphor screen  $V_d$ , the geometrical cross section  $A$  of the grain, as well as on the corresponding absorption ( $Q_{abs}$ ) and scattering ( $Q_{sct}$ ) efficiency factors, which are given below:<sup>36,42,62</sup>

$$Q_{ext} = \frac{2}{x^2} \sum_{n=1}^{\infty} (2n+1) \text{Re}(a_n + b_n), \quad Q_{sct} = \frac{2}{x^2} \sum_{n=1}^{\infty} (2n+1) \times (|a_n|^2 + |b_n|^2). \quad (\text{A2})$$

The geometrical cross section of the grain  $A$  is proportional to the diameter of the grain  $d$  being equal to  $A = \pi d^2/4$ . The extinction and scattering efficiency factors are obtained from Mie calculations using the size parameter  $x = \pi d n_{medium}/\lambda$  of Mie theory and the relative complex refractive index  $m = n_{grain}/n_{medium}$ , where  $\lambda$  is the wavelength of light,  $n_{grain}$  is the complex refractive index of the phosphor grains, and  $n_{medium}$  is the refractive index of the of the me-

dium. Finally,  $a_n$  and  $b_n$  are the so-called Mie coefficients, which are given by the following equations:<sup>42</sup>

$$a_n = \frac{\psi'_n(mx)\psi_n(x) - m\psi_n(mx)\psi'_n(x)}{\psi'_n(mx)\zeta_n(x) - m\psi_n(mx)\zeta'_n(x)},$$

$$b_n = \frac{m\psi'_n(mx)\psi_n(x) - \psi_n(mx)\psi'_n(x)}{m\psi'_n(mx)\zeta_n(x) - \psi_n(mx)\zeta'_n(x)}, \quad (\text{A3})$$

where  $\psi_n(x)$  and  $\zeta_n(x)$  are the Riccati-Bessel functions. The calculation of these functions can be carried out by the following recurrences, taking into account their corresponding properties:

$$\begin{aligned} \psi_{n+1}(x) &= (2n+1)\psi_n(x)/x - \psi_{n-1}(x), \\ \zeta_{n+1}(x) &= (2n+1)\zeta_n(x)/x - \zeta_{n-1}(x), \\ \psi'_n(x) &= \psi_{n-1}(x) - n\psi_n(x)/x, \\ \zeta'_n(x) &= \zeta_{n-1}(x) - n\zeta_n(x)/x, \\ \psi_{-1}(x) &= \cos(x), \quad \psi_0(x) = \sin(x), \\ \zeta_{-1}(x) &= \cos(x) - i \sin(x), \quad \zeta_0(x) = \sin(x) + i \cos(x). \end{aligned} \quad (\text{A4})$$

The infinite summations in relations (A2) for the extinction and scattering efficiency factors calculations converge after a certain number  $N_{max} = x + cx^{1/3} + b$ , where  $c=4$  and  $b=2$  depending on  $x$ . Usually the recursion formulas are used up to  $N_{max}$ th order.

## APPENDIX B: HENY-STEIN DISTRIBUTION

The probability density function of Henyey-Greenstein distribution,<sup>60</sup>  $p(\cos \theta)$ , is given below:

$$p(\cos \theta) = \frac{1 - g^2}{2[1 + g^2 - 2g \cos(\theta)]^{3/2}}, \quad (\text{B1})$$

where  $g$  is the anisotropy factor and corresponds to the mean cosine of the scattering angle.<sup>60</sup> Using the cumulative density function,

$$P(\cos \theta) = \int_{-1}^{\cos \theta} \frac{1 - g^2}{2[1 + g^2 - 2g \cos(\theta)]^{3/2}} d \cos \theta, \quad (\text{B2})$$

the random numbers of  $\cos \theta$  are produced from the following equation:<sup>60</sup>

$$\cos \theta = \frac{1}{2g} \left[ 1 + g^2 - \left( \frac{1 - g^2}{1 - g + 2gR} \right)^2 \right] \quad \text{when } g \neq 0. \quad (\text{B3})$$

The free parameter  $g$  is the anisotropy factor, which implies isotropic distribution of light for  $g=0$  and sharply forward direction of light for  $g=1$ . The anisotropy factor was calculated using the following equation:<sup>42,60</sup>

$$g = \frac{\int_0^\pi 2\pi S_{11}(\theta) \cos \theta \sin \theta d\theta}{\int_0^\pi 2\pi S_{11}(\theta) \sin \theta d\theta}, \quad (\text{B4})$$

where  $S_{11}(\theta)$  is the first element of the Mueller matrix,<sup>42</sup> which implies that light extinction is independent of the light polarization state. In numerical evaluation of the above expression for  $g$ , a large number of angles are required to be calculated in order to obtain a high precision value of  $g$ .  $S_{11}(\theta)$  is associated to the complex elements of scattering matrix  $S_1(\theta)$  and  $S_2(\theta)$  as follows:<sup>41,62</sup>

$$S_{11}(\theta) = |S_1(\theta)|^2 + |S_2(\theta)|^2, \quad (\text{B5})$$

where

$$S_1(\theta) = \sum_{n=1}^{\infty} \frac{2n+1}{n(n+1)} [a_n \pi_n(\cos \theta) + b_n \tau_n(\cos \theta)], \quad (\text{B6})$$

and

$$S_2(\theta) = \sum_{n=1}^{\infty} \frac{2n+1}{n(n+1)} [b_n \pi_n(\cos \theta) + a_n \tau_n(\cos \theta)]. \quad (\text{B7})$$

The angle-dependent functions  $\pi_n$  and  $\tau_n$  were computed by upward recurrence from the following relations:

$$\pi_n = \frac{2n-1}{n-1} \cos \theta \pi_{n-1} - \frac{n}{n-1} \pi_{n-2} \quad (\text{B8a})$$

and

$$\tau_n = n \cos \theta \pi_n - (n+1) \pi_{n-1}, \quad (\text{B8b})$$

beginning with  $\pi_0=0$  and  $\pi_1=1$ .

<sup>a)</sup> Author to whom correspondence should be addressed. Electronic mail: panayiot@upatras.gr

<sup>1</sup> G. F. Knoll, *Radiation Detection and Measurement*, 2nd ed. (Wiley, New York, 1989).

<sup>2</sup> H. E. Johns and J. R. Cunningham, *The Physics of Radiology* (Thomas, Springfield, IL, 1983).

<sup>3</sup> M. J. Yaffe, "Physics and Psychophysics," in *Handbook of Medical Imaging*, edited by J. Beutel, H. L. Kundel, and R. L. Van Metter (SPIE, Bellingham, WA, 2000), Vol. I, Chap. 5, pp. 329–372.

<sup>4</sup> G. Blasse and B. C. Grabmaier, *Luminescent Materials* (Springer, Berlin, 1994).

<sup>5</sup> R. C. Alig and S. Bloom, "Cathodoluminescent Efficiency," *J. Electrochem. Soc.* **124**, 1136–1138 (1977).

<sup>6</sup> S. E. Derenzo, W. W. Moses, J. L. Cahoon, R. C. C. Perera and J. E. Litton, "Prospects for new inorganic scintillators," *IEEE Trans. Nucl. Sci.* **NS-37**, 203–208 (1990).

<sup>7</sup> C. W. E. van Eijk, "Inorganic-scintillator development" *Nucl. Instrum. Methods Phys. Res. A* **460**, 1–14 (2001).

<sup>8</sup> C. E. Dick and J. W. Motz, "Image information transfer properties of x-ray fluorescent screens," *Med. Phys.* **8**, 337–346 (1981).

<sup>9</sup> C. E. Dick and J. W. Motz, "Utilization of monoenergetic x-ray beams to examine the properties of radiographic intensifying screens," *IEEE Trans. Nucl. Sci.* **NS-28**, 1554–1558 (1981).

<sup>10</sup> A. Ginzburg and C. E. Dick, "Image information transfer properties of x-ray intensifying screens in the energy range from 17 to 320 keV," *Med. Phys.* **20**, 1013–1021 (1993).

<sup>11</sup> H. W. Venema, "X-ray absorption, speed and luminescent efficiency of rare earth and other intensifying screens," *Radiology* **130**, 765–771 (1979).

<sup>12</sup> H. P. Chan and K. Doi, "Energy and angular dependence of x-ray absorp-

tion and its effect on radiographic response in screen-film systems," *Phys. Med. Biol.* **28**, 565–579 (1983).

<sup>13</sup> B. Nielsen and C. A. Carlson, "Energy imparted to fluorescent screens from primary and scattered radiation. Variations with atomic composition and screen thickness," *Phys. Med. Biol.* **29**, 315–328 (1984).

<sup>14</sup> R. M. Nishikawa and M. J. Yaffe, "Model of the spatial-frequency-dependent detective quantum efficiency of phosphor screens," *Med. Phys.* **17**, 894–904 (1990).

<sup>15</sup> I. Kandarakis, D. Cavouras, G. S. Panayiotakis, and C. D. Nomicos, "Evaluating x-ray detectors for radiographic applications: A comparison of ZnSCdS:Ag with Gd<sub>2</sub>O<sub>2</sub>S:Tb and Y<sub>2</sub>O<sub>2</sub>S:Tb screens," *Phys. Med. Biol.* **42**, 1351–1373 (1997).

<sup>16</sup> D. E. Raeside, "Monte Carlo principles and applications," *Phys. Med. Biol.* **21**, 181–197 (1976).

<sup>17</sup> R. Y. Rubinstein, *Simulation and the Monte Carlo Method* (Wiley, New York, 1981).

<sup>18</sup> R. L. Morin, *Monte Carlo Simulation in the Radiological Science* (CRC, Boca Raton, FL, 1988).

<sup>19</sup> P. Andreo, "Monte Carlo techniques in medical radiation physics," *Phys. Med. Biol.* **36**, 861–920 (1991).

<sup>20</sup> W. Kalender, "Monte Carlo calculations of x-ray scatter data for diagnostic radiology," *Phys. Med. Biol.* **26**, 835–849 (1981).

<sup>21</sup> H. P. Chan and K. Doi, "The validity of Monte Carlo simulation in studies of scattered radiation in diagnostic radiology," *Phys. Med. Biol.* **28**, 109–129 (1983).

<sup>22</sup> W. Aerts, P. J. De Meester, and R. Bollen, "A Monte Carlo simulation of complete systems for radiographic image registration," *Mater. Eval.* **40**, 1071–1075 (1982).

<sup>23</sup> M. J. Yaffe and J. A. Rowlands, "X-ray detectors for digital radiography," *Phys. Med. Biol.* **42**, 1–39 (1997).

<sup>24</sup> S. M. Gruner, M. W. Tate, and E. F. Eikenberry, "Charge-coupled device area x-ray detectors," *Rev. Sci. Instrum.* **73**, 2816–2842 (2002).

<sup>25</sup> C. W. E. van Eijk, "Inorganic scintillators in medical imaging," *Phys. Med. Biol.* **47**, R85–R106 (2002).

<sup>26</sup> H. Hamaker, "Radiation and heat conduction in light-scattering material," *Philips. Res. Rep.* **2**, 55–67 (1947).

<sup>27</sup> G. W. Ludwig, "X-ray efficiency of powder phosphors," *J. Electrochem. Soc.* **118**, 1152–1159 (1971).

<sup>28</sup> G. W. Ludwig and J. S. Prener, "Evaluation of Gd<sub>2</sub>O<sub>2</sub>S:Tb as a phosphor for the input screen of x-ray image intensifier," *IEEE Trans. Nucl. Sci.* **13**, 3–8 (1972).

<sup>29</sup> R. K. Swank, "Absorption and noise in x-ray phosphors," *J. Appl. Phys.* **45**, 4199–4203 (1974).

<sup>30</sup> G. E. Giakoumakis, C. D. Nomicos, and P. C. Euthimiou, "Modulation transfer function of fluorescent screens excited by x-rays," *Phys. Med. Biol.* **25**, 1105–1110 (1980).

<sup>31</sup> J. Lindstrom and G. A. Carlsson, "A simple model for estimating the particle size dependence of absolute efficiency of fluorescent screens," *Phys. Med. Biol.* **44**, 1353–1367 (1999).

<sup>32</sup> G. E. Giakoumakis, M. C. Katsarioti, I. E. Lagaris, and G. S. Panayiotakis, "A theoretical model for the x-ray luminescence of granular phosphor screens," *J. Appl. Phys.* **69**, 6607–6610 (1991).

<sup>33</sup> J. M. Boone and J. A. Seibert, "A Monte Carlo study of x-ray fluorescence in x-ray detectors," *Med. Phys.* **26**, 905–916 (1999).

<sup>34</sup> D. A. Jaffray, J. J. Battista, A. Fenster, and P. Munro, "Monte Carlo studies of x-ray energy absorption and quantum noise in megavoltage transmission radiography," *Med. Phys.* **22**, 1077–1088 (1995).

<sup>35</sup> B. D. Galas, J. S. Boswell, A. Badano, R. M. Gagne, and K. J. Myers, "An energy- and depth-dependent model for x-ray imaging," *Med. Phys.* **31**, 3132–3149 (2004).

<sup>36</sup> R. Morlotti, "X-ray efficiency and modulation transfer function of fluorescent rare earth screens, determined by the Monte Carlo method," *J. Photogr. Sci.* **23**, 181–189 (1975).

<sup>37</sup> T. Radcliffe, G. Barnea, B. Wowk, R. Rajapakshe, and S. Shalev "Monte Carlo optimization of metal/phosphor screens at megavoltage," *Med. Phys.* **20**, 1161–1169 (1993).

<sup>38</sup> C. Kausch, B. Schreiber, F. Kreuder, R. Schmidt, and O. Dössel "Monte Carlo simulations of the imaging performance of metal plate/phosphor screens used in radiotherapy," *Med. Phys.* **26**, 2113–2124 (1999).

<sup>39</sup> A. Badano, R. M. Gagne, B. D. Gallas, R. J. Jennings, J. S. Boswell, and K. J. Myers, "Lubberts effect in columnar phosphors," *Med. Phys.* **31**, 3122–3131 (2004).

<sup>40</sup> V. V. Nagarkar, S. R. Miller, S. V. Tipnis, A. Lempicki, C. Brecher, and

- H. Lingertat, "A new large area scintillator screen for x-ray imaging," *Nucl. Instrum. Methods Phys. Res. B* **213**, 250–254 (2004).
- <sup>41</sup>C. F. Bohren and D. R. Huffman, *Absorption and Scattering of Light by Small Particles* (Wiley, New York, 1983).
- <sup>42</sup>H. C. Van de Hulst, *Light Scattering by Small Particles* (Wiley, New York, 1957).
- <sup>43</sup>J. M. Boone and A. Seibert, "An accurate method for computer-generating tungsten anode x-ray spectra from 30 to 140 kV," *Med. Phys.* **24**, 1661–1670 (1997). X-ray simulation tool. <http://www.med.siemens.com/med/rv/spektrum/default.asp>
- <sup>44</sup>J. M. Boone, T. R. Fewell, and R. J. Jennings, "Molybdenum, rhodium, and tungsten anode spectral models using interpolating polynomials with application to mammography," *Med. Phys.* **24**, 1863–1874 (1997). X-ray simulation tool. <http://www.med.siemens.com/med/rv/spektrum/default.asp>
- <sup>45</sup>J. M. Boone, "Spectral modeling and compilation of quantum fluence in radiography and mammography," *Proc. SPIE* **3336**, 592–601 (1998). X-ray simulation tool. <http://www.med.siemens.com/med/rv/spektrum/default.asp>
- <sup>46</sup>M. J. Berger, J. H. Hubell, S. M. Seltzer, J. S. Coursey, and D. S. Zucker, "XCOM: Photon cross section database," Technical report, NIST (1999). <http://physics.nist.gov/xcom>.
- <sup>47</sup>H. Zaidi, "Comparative evaluation of photon cross-section libraries for materials of interest in PET Monte Carlo simulations," *IEEE Trans. Nucl. Sci.* **47**, 2722–2735 (2000).
- <sup>48</sup>J. M. Boone and A. E. Chavez, "Comparison of x-ray cross sections for diagnostic and therapeutic medical physics," *Med. Phys.* **23**, 1997–2005 (1996).
- <sup>49</sup>J. H. Hubbell, Wm. J. Veigele, E. A. Briggs, R. T. Brown, D. T. Cromer, and R. J. Howerton, "Atomic form factors, incoherent scattering functions, and photon scattering cross sections," *J. Phys. Chem. Ref. Data* **4**, 471–537 (1975).
- <sup>50</sup>D. E. Cullen, J. H. Hubbell, and L. Kissel, "EPDL97 The evaluated data library, '97 version," Report UCRL-50400, LLNLL, CA (1997).
- <sup>51</sup>J. H. Hubbell, P. N. Trehan, N. Singh, B. Chand, D. Mehta, M. L. Garg, R. R. Grag, S. Singh, and S. Puri, "A review, bibliography, and tabulation of K, L, and higher atomic shell x-ray fluorescence yields," *J. Phys. Chem. Ref. Data* **23**, 339–364 (1994).
- <sup>52</sup>J.-P. Moy, "Recent developments in x-ray imaging detectors," *Nucl. Instrum. Methods Phys. Res. A* **442**, 26–37 (2000).
- <sup>53</sup>G. E. Giakoumakis, C. D. Nomicos, E. N. Yiakoumakis, and E. K. Evangelou, "Absolute efficiency of rare earth oxysulphide screens in reflection mode observation," *Phys. Med. Biol.* **35**, 1017–1023 (1990).
- <sup>54</sup>J. Sempau, E. Acosta, J. Baro, J. M. Fernandez-Varea, and F. Salvat, "An algorithm for Monte Carlo simulation of coupled electron-photon transport," *Nucl. Instrum. Methods Phys. Res. B* **132**, 377–390 (1997).
- <sup>55</sup>D. Brusa, G. Stutz, J. A. Riveros, J. M. Fernandez-Varea, and F. Salvat, "Fast sampling algorithm for the simulation of Compton scattering," *Nucl. Instrum. Methods Phys. Res. A* **379**, 167–175 (1996).
- <sup>56</sup>G. Blasse, "The luminescent efficiency of scintillators for several applications: state-of-the-art," *J. Lumin.* **60&61**, 930–935 (1994).
- <sup>57</sup>R. Morlotti, M. Nicl, M. Piazza, and C. Boragno, "Intrinsic conversion efficiency of X-rays to light in  $\text{Gd}_2\text{O}_2\text{S}:\text{Tb}^{3+}$  powder phosphors," *J. Lumin.* **72–74**, 772–774 (1997).
- <sup>58</sup>J. Beutel, B. A. Apple, and R. Shaw, "The role of screen parameters and print-through in the performance of film/screen systems," *Phys. Med. Biol.* **38**, 1181–1193 (1993).
- <sup>59</sup>J. Beutel and E. L. Kitts, "The image quality characteristics of a novel film/screen system for mammography," *Proc. SPIE* **2708**, 233–240, (1996).
- <sup>60</sup>V. G. Peters, D. R. Wyman, M. S. Patterson, and G. L. Frank, "Optical properties of normal and diseased human breast tissues in the visible and near infrared," *Phys. Med. Biol.* **35**, 1317–1334 (1990).
- <sup>61</sup>R. Graaff, M. H. Koelink, F. F. M. de Mul, W. G. Zijlstra, A. C. M. Dassel, and J. G. Aarmoudse, "Condensed Monte Carlo simulations for the description of light transport," *Appl. Opt.* **32**, 426–434 (1993).
- <sup>62</sup>H. Du, "Mie-scattering calculation," *Appl. Opt.* **43**, 1951–1956 (2004).
- <sup>63</sup>G. E. Giakoumakis and C. D. Nomicos, "Light angular distribution of non-granular fluorescent screens excited by x-rays," *Phys. Med. Biol.* **30**, 993–1003 (1985).
- <sup>64</sup>A. Roos and D. Ronnow, "Diffuse reflectance and transmittance spectra of an interference layer: I. Model formulation and properties," *Appl. Opt.* **33**, 7908–7917 (1994).
- <sup>65</sup>L. Wang, S. L. Jacques, and L. Zheng, "MCML-Monte Carlo modeling of light transport in multi-layered tissues," *Comput. Methods Programs Biomed.* **47**, 131–146 (1995).
- <sup>66</sup>P. C. Bunch, K. E. Huff, and R. Van Metter, "Analysis of the detective quantum efficiency of a radiographic screen-film combination," *J. Opt. Soc. Am. A* **4**, 902–908 (1987).